

Observation of Terahertz Radiation via the Two-Color Laser Scheme with Uncommon Frequency Ratios

Liang-Liang Zhang,¹ Wei-Min Wang,^{2,1,6,*} Tong Wu,³ Rui Zhang,³ Shi-Jing Zhang,³

Cun-Lin Zhang,¹ Yan Zhang,¹ Zheng-Ming Sheng,^{4,5,6,7} and Xi-Cheng Zhang^{8,1}

¹Beijing Advanced Innovation Center for Imaging Technology and Key Laboratory of Terahertz Optoelectronics (MoE),
Department of Physics, Capital Normal University, Beijing 100048, China

²Beijing National Laboratory for Condensed Matter Physics, Institute of Physics, CAS, Beijing 100190, China

³Beijing Key Laboratory for Precision Optoelectronic Measurement Instrument and Technology, School of Optoelectronics,
Beijing Institute of Technology, Beijing 100081, China

⁴SUPA, Department of Physics, University of Strathclyde, Glasgow G4 0NG, United Kingdom

⁵Key Laboratory for Laser Plasmas (MoE) and School of Physics and Astronomy, Shanghai Jiao Tong University,
Shanghai 200240, China

⁶IFSA Collaborative Innovation Center, Shanghai Jiao Tong University, Shanghai 200240, China

⁷Tsung-Dao Lee Institute, Shanghai Jiao Tong University, Shanghai 200240, China

⁸The Institute of Optics, University of Rochester, Rochester, New York 14627, USA

(Received 29 August 2017; published 8 December 2017)

In the widely studied two-color laser scheme for terahertz (THz) radiation from a gas, the frequency ratio of the two lasers is usually fixed at $\omega_2/\omega_1 = 1:2$. We investigate THz generation with uncommon frequency ratios. Our experiments show, for the first time, efficient THz generation with new ratios of $\omega_2/\omega_1 = 1:4$ and $2:3$. We observe that the THz polarization can be adjusted by rotating the longer-wavelength laser polarization and the polarization adjustment becomes inefficient by rotating the other laser polarization; the THz energy shows similar scaling laws with different frequency ratios. These observations are inconsistent with multiwave mixing theory, but support the gas-ionization or plasma-current model. This study pushes the development of the two-color scheme and provides a new dimension to explore the long-standing problem of the THz generation mechanism.

DOI: 10.1103/PhysRevLett.119.235001

Terahertz (THz) waves have broad applications in THz spectroscopy [1,2] and THz-field matter interactions [3,4]. These applications can potentially benefit from powerful THz radiation sources with various parameters via different laser-plasma-based schemes [5–9]. For example, MV/cm-scale THz radiation with either linear [5,10,11] or elliptical polarization [12–15] can be generated from gas plasma. THz radiation of near mJ can be produced via relativistic laser interaction with solid plasma [8,16–18]. Among these schemes, the two-color laser scheme [5] has been studied most widely [19–28] because it can provide high-efficiency tabletop broadband sources. Generally, an 800-nm pump laser pulse passes through a frequency-doubling crystal to generate a second-harmonic pulse and then the two pulses are mixed to produce gas plasma. Up to now, the frequency ratio of the two-color pulses has always been taken as $\omega_2/\omega_1 = 1:2$ in experiments, although the fundamental-pulse wavelength longer than 800 nm was adopted in recent experiments to enhance the THz strength [29–31] and the second-harmonic-pulse frequency was detuned to yield ultrabroadband radiation [32]. Since 2013, a few theoretical reports [33–35] have predicted that the two-color scheme could be extended to uncommon frequency ratios such as $\omega_2/\omega_1 = 1:4$, $2:3$, but these predictions have not yet been verified experimentally.

In this Letter, we present the first experimental demonstration of THz generation with uncommon frequency ratios. With the ω_1 -laser wavelength fixed at 800 and 400 nm, respectively, a scan of the ω_2 -laser wavelength from 1200 to 1600 nm shows that the THz energies have three resonantlike peaks located near $\omega_2/\omega_1 = 1:4$, $1:2$, and $2:3$. The energies at these peaks are at the same order. Beyond the previous predictions [33–35], we find that the THz polarization can be adjusted by rotating the ω_2 -pulse polarization and, however, the polarization adjustment becomes inefficient by rotating the ω_1 -pulse polarization. In this Letter, we define the ω_1 pulse as the higher-frequency one. These observations agree with our particle-in-cell (PIC) simulations and a model based on field ionization.

The current experiments with the new frequency ratios also provide a new dimension to explore further the THz-generation mechanism. Since 2000, it has been a frequently discussed topic: whether this THz generation can be attributed to multiwave mixing [5,10,36], field ionization (or plasma current) [11,20,37], or to both [27,31]. First, multiwave mixing theory predicts that the THz energy ϵ_{THz} scales with $(P_1)(P_2)^2$ in the original scheme, where P_1 and P_2 are powers of the two pulses. With $\omega_2/\omega_1 = 1:4$ and $2:3$, ϵ_{THz} should follow different

scaling laws $(P_1)(P_2)^4$ and $(P_1)^2(P_2)^3$, respectively. In the experiments, we observe complex dependence of ε_{THz} on P_1 and P_2 that is similar with different ω_2/ω_1 , in disagreement with these scaling laws. Second, we observe that the THz polarization varies only with rotating the polarization of the longer-wavelength laser, which is inconsistent with the symmetric nature in the susceptibility tensor required by the multiwave mixing theory [10].

Experimental setup.—Figure 1(a) shows a schematic of our experiment. The laser pulse is delivered from a Ti:sapphire amplifier (Spitfire, Spectra Physics) with a central wavelength 800 nm, duration 50 fs, and repetition rate 1 kHz. The pulse with total energy 5.3 mJ is split into two parts. The part with 3.5 mJ is used to pump an optical parametric amplifier (TOPAS), which delivers a pulse wavelength tunable from 1200 to 1600 nm (the ω_2 pulse). The remaining energy is used as the ω_1 pulse of the 800-nm wavelength [see Fig. 1(c) as an example]. In another group of experiments [see Fig. 1(d)], the 800-nm pulse passes through a switchable β -barium borate (BBO) crystal and bandpass filter to generate a 400-nm-wavelength pulse (the ω_1 one). The ω_1 and ω_2 pulses propagate collinearly using a dichromatic mirror and have a confocal spot focused by

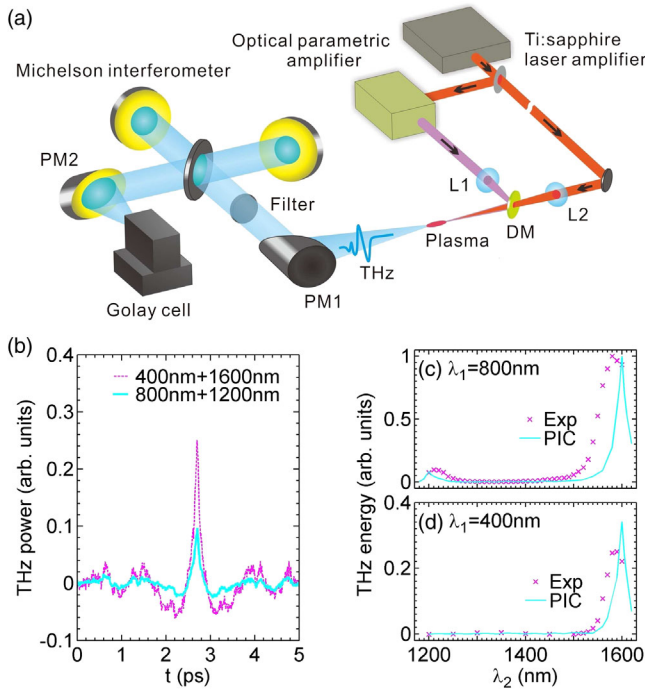


FIG. 1. (a) Experimental setup. L, lens; DM, dichromatic mirror; PM, parabolic mirrors. (b) THz waveforms with $\omega_2/\omega_1 = 1:4$ and $2:3$, respectively, obtained from the autocorrelation measurements, in which the THz powers are normalized by the one with the 800- and 1600-nm pulses. (c), (d) THz energy as a function of the second pulse wavelength λ_2 , where the first pulse wavelength λ_1 is fixed as 800 nm in (c) and 400 nm in (d). Powers of the two pulses are taken as $P_1 = 120$ mW and $P_2 = 400$ mW in (c) and $P_1 = 180$ mW and $P_2 = 250$ mW in (d).

two convex lenses with equal focal length $f = 12.5$ cm. Both pulses are linearly polarized in the horizontal plane initially and their polarizations can be independently controlled by half-wave plates. Powers can also be independently adjusted through optical attenuators. The two pulses irradiate air and produce a few millimeters of plasma.

We use an off-axis parabolic mirror to collect and collimate the forward THz radiation from the air plasma after eliminating the pump laser pulses with a long-pass THz filter (Tydex Ltd.). To measure the horizontal and vertical components of the radiation, a wire grid polarizer is employed. A Golay THz detector with a 6-mm diameter diamond input window (Microtech SN:220712-D) is used to measure the radiation energy, where the detector shows a nearly flat response in the spectral range from 0.1 to 150 THz. The voltage signal is fed into a lock-in amplifier referenced to a 15-Hz modulation frequency. To obtain the THz radiation bandwidth, autocorrelation measurement is carried out by a Michelson interferometer containing a silicon wafer.

Experimental and PIC simulation results.—We first present the experimental and PIC simulation results in Figs. 1–3 and then explain them with a theoretical model. First, the measured THz waveforms plotted in Fig. 1(b) show that the THz peak powers with $\omega_2/\omega_1 = 1:4$ and $2:3$ are about 30% and 10% compared with $\omega_2/\omega_1 = 1:2$. By scanning ω_2 from 1200 to 1600 nm, we observe that the THz radiation can be effectively generated only around $\omega_2/\omega_1 = 2:3$ and $1:2$ in Fig. 1(c) with the ω_1 pulse of

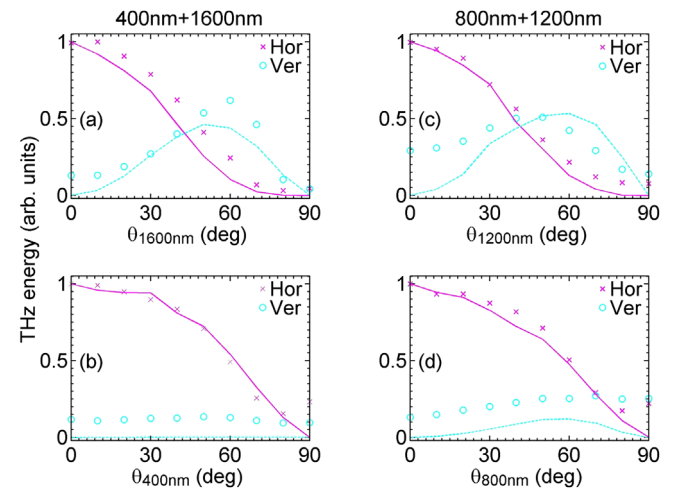


FIG. 2. THz energies of the horizontal and vertical components as a function of the rotation angle θ of the field polarization of (a) the 1600-nm pulse, (b) 400-nm pulse, (c) 1200-nm pulse, and (d) 800-nm pulse, respectively, where when polarization of one pulse is rotated, polarization of the other pulse is fixed at the horizontal. Experimental results are shown by crosses and circles and PIC results by lines. The left-hand column corresponds to the case with the 400-nm (with 180 mW) and 1600-nm (250 mW) pulses and the right-hand column to the case with the 800-nm (120 mW) and 1200-nm (400 mW) pulses.

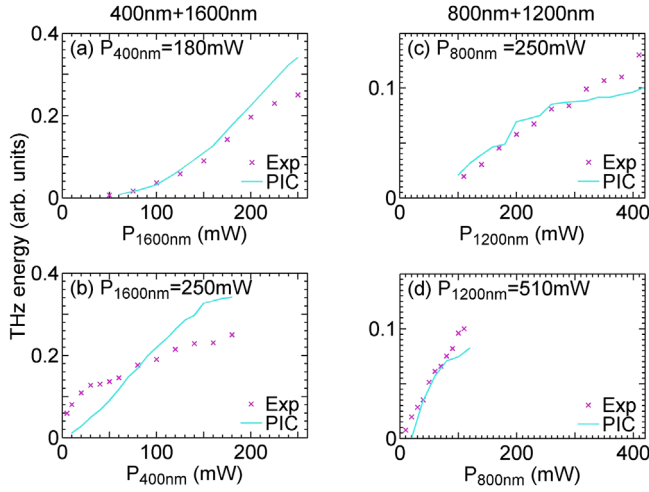


FIG. 3. THz energy as a function of the power of (a) the 1600-nm pulse, (b) 400-nm pulse, (c) 1200-nm pulse, and (d) 800-nm pulse, respectively, where when the power of one pulse is changed, the power of the other pulse is fixed. The left-hand column corresponds to the case with the 400- and 1600-nm pulses and the right-hand column to the case with the 800- and 1200-nm pulses.

800 nm as well as around $\omega_2/\omega_1 = 1:4$ in Fig. 1(d) with the ω_1 pulse of 400 nm. Note that these THz peaks have small shifts (10–20 nm in wavelength) from the ones exactly at $\omega_2/\omega_1 = 1:4, 2:3,$ and $1:2$ obtained in the PIC results, which could be caused by inaccuracy of laser wavelengths output from TOPAS. Second, we observe in Fig. 2 that the THz polarization can be adjusted by rotating the polarization of the ω_2 pulse, but the polarization adjustment becomes inefficient by rotating the ω_1 -pulse polarization. This is observed in all the cases of $\omega_2/\omega_1 = 1:4$ [Figs. 2(a) and 2(b)], $\omega_2/\omega_1 = 2:3$ [Figs. 2(c) and 2(d)], and $\omega_2/\omega_1 = 1:2$. For example, with $\omega_2/\omega_1 = 1:4$, when the 1600-nm-pulse polarization is rotated from the horizontal to the vertical in Fig. 2(a), the THz horizontal component is weakened continuously and the vertical component is first strengthened and then weakened, as observed in previous experiments [30] with $\omega_2/\omega_1 = 1:2$. However, when the 400-nm-pulse polarization is rotated in Fig. 2(b), the THz vertical component is kept at a low level close to that at $\theta = 0$ and 90° , which is expected to be at noise level. These observations are reproduced by our PIC simulations. Third, the dependence of the THz energy upon the laser powers does not obey the scaling laws predicted by the multiwave mixing theory, as seen in Fig. 3. The curves in this figure illustrate complex dependence in both cases $\omega_2/\omega_1 = 1:4$ and $2:3$ and each curve in the starting stage appears as a linear dependence, in reasonable agreement with the PIC results.

The agreement between the PIC (near-field radiation) and experimental results (far-field radiation) suggests that the far-field radiation should be mainly contributed from a short gas-plasma zone in which the pulses have the highest

intensities, as modeled in our PIC simulations. In our simulations, we employ a 0.6-mm-long nitrogen to save computational time. We adopt the same laser parameters as in the experiments and assume that on the gas front end the pulses just reach the highest intensities (at the order of 10^{14} W/cm²) and have the spot radius $50 \mu\text{m}$. Our simulations are performed with the KLAPS code [38], which can give near-field radiation with very few approximations [35]. Note that the far-field radiation is composed of all near-field sources [23,24,28]. A simplified near-field model was used to explain THz-generation experiments in Ref. [30].

Theoretical model.—To interpret the PIC and experimental results, we present a theoretical analysis based on a plasma current model. First, Kim *et al.* [11,19] proposed that asymmetric field ionization causes current formation. Then, Wang and co-workers proposed a near-field model including the current dynamics in plasma [15,20,39]. The THz generation includes two processes: net-current formation via field ionization, which lasts shorter than the laser duration 50 fs, and radiation generation as the current is modulated by the plasma, which is at a time scale of 1 ps. Therefore, one can calculate the two processes respectively. The net current $\mathbf{J}_0 = -en_e\mathbf{v}_0$ can be given by

$$\mathbf{J}_0 = \frac{e^2 n_e \mathbf{A}_L(\psi_0)}{m_e c}, \quad (1)$$

where $\mathbf{v}_0 = -e\mathbf{A}_L(\psi_0)/m_e c$, \mathbf{A}_L is the laser vector potential, $\psi = t - z/c$, and ψ_0 is the position where electrons are created. Note that nearly all electrons are periodically created at the same relative position in different periods of the laser fields in the cases $\omega_2/\omega_1 = 1:4, 1:2, 2:3,$ respectively, as shown in Ref. [35]. The electron density is given according to $\partial n_e/\partial t = (n_a - n_e)w(E_L)$, where $w(E_L)$ is the ionization rate [40–42] in the laser field amplitude E_L and n_e and n_a are the electron and initial atom densities, respectively. After passage of the laser pulses, the generated radiation interacts with the current, the electron velocity becomes $\mathbf{v} = \mathbf{v}_0 + e\mathbf{A}_{\text{THz}}/m_e c$, and consequently the current turns to $\mathbf{J} = \mathbf{J}_0 - e^2 n_e \mathbf{A}_{\text{THz}}/m_e c$. Then, the THz radiation can be described by

$$\left(\nabla^2 - \frac{1}{c^2} \frac{\partial^2}{\partial t^2} - \frac{\omega_p^2}{c^2} \right) \mathbf{A}_{\text{THz}} = -4\pi \mathbf{J}_0/c, \quad (2)$$

where $\omega_p = \sqrt{4\pi e^2 n_e/m_e}$ is the plasma oscillation frequency. Equation (2) is difficult to analytically solve since the pulse length of the radiation is longer than the spot size ($\sim 50 \mu\text{m}$) and a one-dimensional approximation [39] cannot be taken. In the following, we will show that numerical calculation of Eq. (1) and simple analysis of Eq. (2) can explain the experimental results above.

Dependence on laser-frequency ratio.—From Eqs. (1) and (2), one can obtain the THz amplitude $A_{\text{THz}} \propto J_0 \propto A_L(\psi_0)$. THz energy peaks appear at peaks of

$A_L(\psi_0)$. Our calculation shows three resonancelike peaks of $A_L(\psi_0)$ located at $\omega_2/\omega_1 = 1:4, 1:2, 2:3$. To quantitatively compare the THz energies at the peaks, we also calculate J_0 , which depends on both $A_L(\psi_0)$ and n_e . Calculating J_0 by Eq. (1) gives the values of J_0 as $0.29:1:(-0.58)$. Then, the THz energies are $0.084:1:0.34$, which is in agreement with the experimental results of $0.097:1:0.26$ as seen in Figs. 1(c) and 1(d). Note that no THz generation with $\omega_2/\omega_1 = 1:3$ can be explained by ionization symmetry [33] while this symmetry can be broken with $\omega_2/\omega_1 = 2:3, 1:4$, etc. [35].

Dependence on laser polarization.—According to Eqs. (1) and (2), the radiation should have only the x component if the two pulses have the same polarization along the x direction. Once the polarization of one pulse is rotated to have the y component, the radiation could have both x and y components. We take the laser electric fields as $E_{L,x} = f(\psi)[a_1 \sin(\omega_1\psi) + a_2 \cos(\theta) \sin(\omega_2\psi)]$ and $E_{L,y} = f(\psi)a_2 \sin(\theta) \sin(\omega_2\psi)$, where θ is the rotation angle and $f(\psi)$ is the envelope profile. The vector potential can be written by $A_{L,x} = cf(\psi)[a_1 \cos(\omega_1\psi)/\omega_1 + a_2 \cos(\theta) \cos(\omega_2\psi)/\omega_2]$ and $A_{L,y} = cf(\psi)a_2 \sin(\theta) \cos(\omega_2\psi)/\omega_2$, since $\partial f(\psi)/\partial\psi \ll \omega_1$ and ω_2 . Electrons are created at $\partial|E_L|/\partial\psi = 0$, which gives $\omega_2\psi_0 = 1.937$ for $\theta = 0$. Our calculation shows that ψ_0 varies slightly with the change in θ . This is because $\partial[\partial|E_L|/\partial\psi]/\partial[\cos(\theta)] \approx 0.06$, with $\omega_2\psi_0 = 1.937$, suggesting that when $\cos(\theta)$ is changed from 1 to 0 (θ from 0 to $\pi/2$), $(\partial|E_L|/\partial\psi)|_{\psi_0+\epsilon} = 0$ is always satisfied if ψ_0 is shifted by a small value ϵ .

Therefore, both $|E_L(\psi_0)|$ and $|A_{L,x}(\psi_0)|$ decreases as θ is increased from 0 to $\pi/2$, where $A_{L,x}(\psi_0) < 0$ and $\cos(\omega_2\psi_0) < 0$. The decrease of $|E_L(\psi_0)|$ and $|A_{L,x}(\psi_0)|$ leads to a reduction of ionization rates and net velocities of electrons, respectively, which can explain the weakening THz horizontal component with θ in Fig. 2(a). This figure also shows that the vertical component is first strengthened from zero and then weakened, which is caused by the increasing $|A_{L,y}(\psi_0)|$ and decreasing $|E_L(\psi_0)|$ with θ . The peak of the vertical component is observed about $\theta = 60^\circ$ approaching the PIC result. Our simulations show the optimized θ within 40° – 70° depends on the laser intensities and frequencies, determined by the balancing point of increasing $|A_{L,y}(\psi_0)|$ and decreasing $|E_L(\psi_0)|$.

In Fig. 2(b) the 400-nm-pulse polarization is rotated, and the THz vertical component is kept at a low level (noise level in the experiments and near zero in the PIC simulations). Rotating either ω_1 or ω_2 pulse, one gets the same $|E_L|$. Consequently, $\partial|E_L|/\partial\psi = 0$ gives the same $\omega_2\psi_0 = 1.937$ for $\theta = 0$ and ψ_0 varies slightly with θ . Therefore, the horizontal component in Fig. 2(b) shows a similar dependence to Fig. 2(a) for the same reason addressed previously. However, the vertical component depends strongly on the laser frequency. When rotating the ω_1 pulse,

$A_{L,y}^{\omega_1}(\psi_0) = cf(\psi_0)a_1 \sin(\theta) \cos(\omega_1\psi_0)/\omega_1$. While rotating the ω_2 pulse, $A_{L,y}^{\omega_2}(\psi_0) = cf(\psi_0)a_2 \sin(\theta) \cos(\omega_2\psi_0)/\omega_2$. One can obtain

$$\frac{A_{L,y}^{\omega_1}(\psi_0)}{A_{L,y}^{\omega_2}(\psi_0)} \approx -\left(\frac{\omega_2}{\omega_1}\right)^2 = -\left(\frac{\lambda_1}{\lambda_2}\right)^2, \quad (3)$$

where we have used $a_1\omega_1 \cos(\omega_1\psi_0) = -a_2\omega_2 \cos(\omega_2\psi_0)$ derived from $\partial|E_L|/\partial\psi = 0$ with $\theta = 0$ since ψ_0 slightly depends upon θ . According to Eq. (3), the vertical THz energy is decreased to $1/256$ when the rotated pulse is changed from the ω_2 one to the ω_1 with $\omega_2/\omega_1 = 1:4$; and the THz energy is decreased to $16/81$ with $\omega_2/\omega_1 = 2:3$. These are in good agreement with our PIC results as shown in Figs. 2(b) and 2(d). Since such low levels of THz energies cannot be resolved in our experiments, the vertical component is observed to be nearly unchanged with varying θ . Similar results are also observed when the 800- and 1600-nm pulses are used.

Note that the observed THz-polarization dependence is inconsistent with the multiwave mixing model [10]. For example, with $\omega_2/\omega_1 = 1:4$, the fifth-order susceptibility tensor χ has $\chi_{xyyyy}^x = \chi_{yxxxx}^y$ because of the symmetry, where the superscript represents the THz polarization and the subscripts represent the polarization of the ω_1 wave and the four ω_2 waves, respectively. $\chi_{xyyyy}^x = \chi_{yxxxx}^y$ requires that the horizontal THz component in Fig. 2(a) should have the same level as the vertical THz component in Fig. 2(b). In contrast, Figs. 2(a) and 2(b) give $\chi_{xyyyy}^x \gg \chi_{yxxxx}^y$. Additionally, both our PIC and experimental results show obvious differences from $\cos^2(\theta)$ scaling for the horizontal component and $\sin(2\theta)$ for the vertical component, which was derived under the different condition $a_1 \ll a_2$ and with $\omega_2/\omega_1 = 1:2$ [30].

Dependence on laser power.—Figure 3 shows complex dependence of the THz energy on the laser power for $\omega_2/\omega_1 = 1:4$ and $2:3$, which significantly deviates from the scaling of $(P_1)(P_2)^4$ and $(P_1)^3(P_2)^2$ predicted by the multiwave mixing theory. This can be attributed to complex dependence of the ionization rates on the laser intensities since the intensities span 1–2 orders of magnitude, which adds complexity to the theoretical analysis. The analysis becomes simpler when the power of one pulse is changed in a low level within $[P_a, P_b]$ and the power of the other pulse is fixed at a much higher value P_c ($P_c \gg P_b$), where the ionization rate and the ionization position ψ_0 vary slightly. This is the case in the starting stage in each curve in Fig. 3. According to $(\partial|E_L|/\partial\psi)(\psi_0) = 0$ for the two pulses with the same polarization, one can obtain $A_{L,x}(\psi_0) = a_1cf(\psi_0) \cos(\omega_1\psi_0)[1/\omega_1 - \omega_1/\omega_2^2]$ or $A_{L,x}(\psi_0) = a_2cf(\psi_0) \cos(\omega_2\psi_0)[1/\omega_2 - \omega_2/\omega_1^2]$. Therefore, $|A_{L,x}(\psi_0)|$ is linearly proportional to a_1 or a_2 . This linear dependence is observed within the starting stage in each

curve in Fig. 3 with either $\omega_2/\omega_1 = 1:4$ or $2:3$ (one can also observe similar results in previous experiments with $\omega_2/\omega_1 = 1:2$ [30]). Note that the PIC and experimental results are not in precise agreement. In the PIC simulations we assume that the laser pulses with different powers have the same spot radius of $50 \mu\text{m}$ when they reach the highest intensities. However, the spot radius will depend on the power, and unfortunately, exploration of this complex dependence is beyond the scope of this work.

In summary, we have experimentally shown that the two-color scheme can still work when ω_2/ω_1 of $1:2$ is changed to $1:4$ and $2:3$. The THz polarization can be adjusted more efficiently by rotating the polarization of the longer-wavelength pulse from the horizontal to the vertical because the THz vertical component follows a fourth-power law of the laser wavelength, which is inconsistent with the multiwave mixing theory. We have observed a complex dependence of the THz energy when the power of one of the two pulses is varied over a large range. A linear dependence with different ω_2/ω_1 has also been observed when the power of one pulse is varied within a limited range much lower than the power of the other pulse. These dependencies disagree with the scaling laws given by the multiwave mixing theory. These observations have been well explained by our PIC simulations and a plasma-current model.

We thank Prof. Yu-Tong Li and David R. Jones for useful discussion. This work was supported by Science Challenge Project of China (Grant No. TZ2016005), the National Basic Research Program of China (Grants No. 2014CB339806, No. 2014CB339801, and No. 2013CBA01500), the National Natural Science Foundation of China (Grants No. 11375261, No. 11775302, and No. 11374007), and the Strategic Priority Research Program of the Chinese Academy of Sciences (Grants No. XDB16010200 and No. XDB07030300). Z.-M. S. acknowledges the support of a Leverhulme Trust Research Grant at the University of Strathclyde and UK Engineering and Physical Sciences Research Council (Grant No. EP/N028694/1). X.-C. Z. was also partially sponsored by the Army Research Office and was accomplished under Grant No. US ARMY W911NF-17-1-0428. Numerical calculations were performed on the Tianhe-2 platform at the National Supercomputer Center in Guangzhou.

*To whom all correspondence should be addressed.
weiminwang1@126.com, hbwwm1@iphy.ac.cn

- [1] B. Clough, J. Dai, and X.-C. Zhang, *Mater. Today* **15**, 50 (2012).
- [2] P. Gaal, W. Kuehn, K. Reimann, M. Woerner, T. Elsaesser, and R. Hey, *Nature (London)* **450**, 1210 (2007).
- [3] T. Kampfrath, K. Tanaka, and K. Nelson, *Nat. Photonics* **7**, 680 (2013).

- [4] S. Spielman, B. Parks, J. Orenstein, D. T. Nemeth, F. Ludwig, J. Clarke, P. Merchant, and D. J. Lew, *Phys. Rev. Lett.* **73**, 1537 (1994).
- [5] D. J. Cook and R. M. Hochstrasser, *Opt. Lett.* **25**, 1210 (2000).
- [6] C. D'Amico, A. Houard, M. Franco, B. Prade, A. Mysyrowicz, A. Couairon, and V. T. Tikhonchuk, *Phys. Rev. Lett.* **98**, 235002 (2007).
- [7] Z.-M. Sheng, K. Mima, J. Zhang, and H. Sanuki, *Phys. Rev. Lett.* **94**, 095003 (2005).
- [8] A. Gopal, S. Herzer, A. Schmidt, P. Singh, A. Reinhard, W. Ziegler, D. Brommel, A. Karmakar, P. Gibbon, U. Dillner *et al.*, *Phys. Rev. Lett.* **111**, 074802 (2013).
- [9] Z. Jin, Z. L. Chen, H. B. Zhuo, A. Kon, M. Nakatsutsumi, H. B. Wang, B. H. Zhang, Y. Q. Gu, Y. C. Wu, B. Zhu, L. Wang, M. Y. Yu, Z. M. Sheng, and R. Kodama, *Phys. Rev. Lett.* **107**, 265003 (2011).
- [10] X. Xie, J. Dai, and X.-C. Zhang, *Phys. Rev. Lett.* **96**, 075005 (2006).
- [11] K. Y. Kim, J. H. Glowina, A. J. Taylor, and G. Rodriguez, *Opt. Express* **15**, 4577 (2007).
- [12] H. C. Wu, J. Meyer-ter-Vehn, and Z. M. Sheng, *New J. Phys.* **10**, 043001 (2008).
- [13] J. Dai, N. Karpowicz, and X.-C. Zhang, *Phys. Rev. Lett.* **103**, 023001 (2009).
- [14] H. Wen and A. M. Lindenberg, *Phys. Rev. Lett.* **103**, 023902 (2009).
- [15] W.-M. Wang, P. Gibbon, Z.-M. Sheng, and Y.-T. Li, *Phys. Rev. Lett.* **114**, 253901 (2015).
- [16] G. Q. Liao *et al.*, *Phys. Rev. Lett.* **114**, 255001 (2015).
- [17] G.-Q. Liao, Y.-T. Li, Y.-H. Zhang, H. Liu, X.-L. Ge, S. Yang, W.-Q. Wei, X.-H. Yuan, Y.-Q. Deng, B.-J. Zhu, Z. Zhang, W.-M. Wang, Z.-M. Sheng, L.-M. Chen, X. Lu, J.-L. Ma, X. Wang, and J. Zhang, *Phys. Rev. Lett.* **116**, 205003 (2016).
- [18] Z. Jin, H. B. Zhuo, T. Nakazawa, J. H. Shin, S. Wakamatsu, N. Yugami, T. Hosokai, D. B. Zou, M. Y. Yu, Z. M. Sheng, and R. Kodama, *Phys. Rev. E* **94**, 033206 (2016).
- [19] K. Y. Kim, A. J. Taylor, J. H. Glowina, and G. Rodriguez, *Nat. Photonics* **2**, 605 (2008).
- [20] W.-M. Wang, Z.-M. Sheng, H.-C. Wu, M. Chen, C. Li, J. Zhang, and K. Mima, *Opt. Express* **16**, 16999 (2008).
- [21] Y. Chen, T.-J. Wang, C. Marceau, F. Theberge, M. Chateaufneuf, J. Dubois, O. Kosareva, and S. L. Chin, *Appl. Phys. Lett.* **95**, 101101 (2009).
- [22] T.-J. Wang, Y. Chen, C. Marceau, F. Theberge, M. Chateaufneuf, J. Dubois, and S. L. Chin, *Appl. Phys. Lett.* **95**, 131108 (2009).
- [23] I. Babushkin, W. Kuehn, C. Kohler, S. Skupin, L. Berge, K. Reimann, M. Woerner, J. Herrmann, and T. Elsaesser, *Phys. Rev. Lett.* **105**, 053903 (2010).
- [24] I. Babushkin, S. Skupin, A. Husakou, C. Kohler, E. Cabrera-Granado, L. Berge, and J. Herrmann, *New J. Phys.* **13**, 123029 (2011).
- [25] Y. S. You, T. I. Oh, and K. Y. Kim, *Phys. Rev. Lett.* **109**, 183902 (2012).
- [26] P. Gonzalez de Alaiza Martinez, I. Babushkin, L. Berge, S. Skupin, E. Cabrera-Granado, C. Kohler, U. Morgner, A. Husakou, and J. Herrmann, *Phys. Rev. Lett.* **114**, 183901 (2015).

- [27] V. A. Andreeva, O. G. Kosareva, N. A. Panov, D. E. Shipilo, P. M. Solyankin, M. N. Esaulkov, P. Gonzalez de Alaiza Martinez, A. P. Shkurinov, V. A. Makarov, L. Berge, and S. L. Chin, *Phys. Rev. Lett.* **116**, 063902 (2016).
- [28] Z. Zhang, Y. Chen, M. Chen, Z. Zhang, J. Yu, Z. Sheng, and J. Zhang, *Phys. Rev. Lett.* **117**, 243901 (2016).
- [29] M. Clerici, M. Peccianti, B. E. Schmidt, L. Caspani, M. Shalaby, M. Giguere, A. Lotti, A. Couairon, F. Legare, T. Ozaki, D. Faccio, and R. Morandotti, *Phys. Rev. Lett.* **110**, 253901 (2013).
- [30] N. V. Vvedenskii, A. I. Korytin, V. A. Kostin, A. A. Murzanev, A. A. Silaev, and A. N. Stepanov, *Phys. Rev. Lett.* **112**, 055004 (2014).
- [31] L. Berge, S. Skupin, C. Kohler, I. Babushkin, and J. Herrmann, *Phys. Rev. Lett.* **110**, 073901 (2013).
- [32] M. D. Thomson, V. Blank, and H. G. Roskos, *Opt. Express* **18**, 23173 (2010).
- [33] W.-M. Wang, Y.-T. Li, Z.-M. Sheng, X. Lu, and J. Zhang, *Phys. Rev. E* **87**, 033108 (2013).
- [34] V. A. Kostin, I. D. Laryushin, A. A. Silaev, and N. V. Vvedenskii, *Phys. Rev. Lett.* **117**, 035003 (2016).
- [35] W.-M. Wang, Z.-M. Sheng, Y.-T. Li, Y. Zhang, and J. Zhang, *Phys. Rev. A* **96**, 023844 (2017).
- [36] K. Liu, A. D. Koulouklidis, D. G. Papazoglou, S. Tzortzakis, and X.-C. Zhang, *Optica* **3**, 605 (2016).
- [37] D. Zhang, Z. Lu, C. Meng, X. Du, Z. Zhou, Z. Zhao, and J. Yuan, *Phys. Rev. Lett.* **109**, 243002 (2012).
- [38] W.-M. Wang, P. Gibbon, Z.-M. Sheng, and Y.-T. Li, *Phys. Rev. E* **91**, 013101 (2015).
- [39] W.-M. Wang, S. Kawata, Z.-M. Sheng, Y.-T. Li, and J. Zhang, *Phys. Plasmas* **18**, 073108 (2011).
- [40] M. V. Ammosov, N. B. Delone, and V. P. Krainov, *Sov. Phys. JETP* **64**, 1191 (1986).
- [41] B. M. Penetrante and J. N. Bardsley, *Phys. Rev. A* **43**, 3100 (1991).
- [42] G. Gibson, T. S. Luk, and C. K. Rhodes, *Phys. Rev. A* **41**, 5049 (1990).